Training toward Advanced 3D Seismic Methods for CO2 Monitoring, Verification, and Accounting

Type of Report: Progress

Frequency of Report: Quarterly

Reporting Period: April 1, 2011 – June 30, 2011

DOE Award Number: DE-FE002186 (UH budget G091836)

Submitting Organizations: Department of Earth and Atmospheric Sciences
Allied Geophysical Lab
University of Houston
Houston, Texas 77004-5505

Preparers: **Prof. Christopher Liner – P.I.**
Phone: (713) 743-9119
Fax: (713) 748-7906
Dr. Jianjun Zeng (research scientist)
Dr. Po Geng (research scientist)
Qiong Wu (Ph.D. candidate)
Jintan Li (Ph.D. candidate)
Johnny Seales (ugraduate) … coordinator for this report
Tim Brown (MS candidate)
Eric Swanson (MS candidate)

Distribution List:

FITS	FITS@netl.doe.gov	DOE-NETL
Karen Cohen	Karen.Cohen@netl.doe.gov	DOE-NETL
Vanessa Stepney	Vstepney@central.uh.edu	UH Contracts Office
Jack Casey	jfcasey@uh.edu	UH EAS Department Chair
Laura Bell	lbell4@uh.edu	UH EAS Department Admin
June Zeng	jzeng2007@gmail.com	Team Member
Qiong Wu	qiongwu2010@gmail.com	Team Member
Johnny Seales	Johnny.seales@gmail.com	Team Member
Lee Bell	lee.bell@geokinetics.com	Geokinetics (Industrial partner)
Keith Matthews	kmatthews@fairfield.com	Fairfield (Industrial partner)
Subhashis Mallick	smallick@uwyo.edu	Univ. of Wyoming
Steve Stribling	SStribling@gmocks.com	Grand Mesa Production

CONTENTS

Executive Summary

This report presents major advances in progress made through the reporting period the CO_2 sequestration training project in the Dickman field, Ness County, Kansas.

We continue to investigate narrow band seismic images (41 Hz) that indicate additional channel features not seen in broadband data. In this quarter we have made progress validating them.

As part of undergraduate J. Seales training program, we have teamed up with a group in the Allied Geophysical Lab at the University of Houston who are making ultrasonic transmission measurements to estimate P and S wave speed in calibration material (aluminum). In this work, time-of-flight is used to estimate wave speed, but an important problem is accurate picking of the P-wave first arrival times and later S-wave arrival times. New methods are reported for first break picking.

Looking ahead to numerical modeling based on layer models from well logs, we performed tests related to numerical dispersion, a kind of undesirable noise or artifact that develops in numerical modeling of wave fields. We give a discussion and examples of how to minimize numerical dispersion.

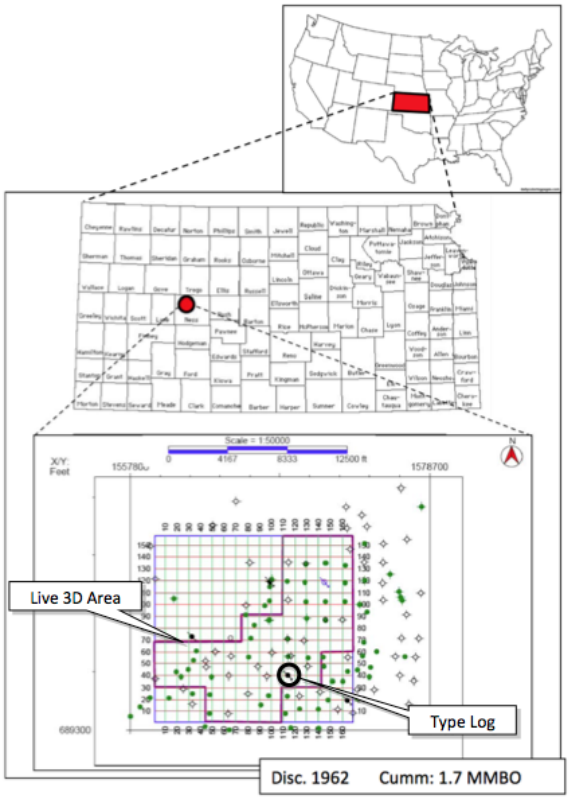

3D Seismic
- 3.325 sq.mi.

142 wells
- 54 in 3D area
- 45 with digital logs
  - GR (43), Resistivity (25), Neutron (27), P-Sonic (6), Density (3)
- 7 with core
  - porosity and permeability
- 3 full deep saline aquifer penetration

Narrow-band channel interpretation

We continue to investigate narrow band seismic images (41 Hz) that indicate additional channel features not seen in broadband data. As seen in Figure 1, the Mildred Schaben 3 well (MS3) is located to the East and lies adjacent to the intersection of what appears to be a connecting point for two tributaries feeding toward the main channel. The Schaben C2 well (SC2) lies just to the West of where the now single tributary is located. Farther North, notice the Humphrey 1 well (H1) lies outside the tributary and main channel. This gives a basis for comparison of H1 logs with others lying in or very close to the channel and its extension. Finally, the Elmore 2 well (E2), lies directly in the middle of the main channel. This is a good indicator of what log responses we should expect to see in MS3 and SC2 if in fact the extensional channel feature is present.

The cross section of Figure 1 is shown in detail in Figure 2, each well is represented by resistivity (RES) and gamma ray (GR) log curves across the Mississippian-Pennsylvanian (MP) boundary. This reveals a succession of fining upwards sequences, typical of channel fill deposits (Boggs, 2006), indicated by GR as we move between MS3, SC2, and E2. The H1 well does not exhibit this same character in the section of log data available, but the sequences may be present below total depth of this well. Notice the similarity within the resistivity logs of MS3, SC2, and E2. Once attention is shifted to the H1 resistivity log, notice this well does not have the same response pattern as the others.

We can see a general trend that indicated with blue arrows, showing fining upwards sequences that are then truncated above by a coarser member. Fine and course refer to sediment grain size. If we consider these successions, it is possible to locate three main areas of interest. The first is located near the base of the logs where our first truncation occurs and is visible in each log. The second location of interest is indicated by the highest of the three blue dashed lines. This is where the fining upwards sequences appear to end and the logs begin to register events in a more oscillatory manner. The middle of the three blue dashed lines appears to only be present in SC2 and E2. This shows we have a higher energy environment moving from West to East along our wells that lie within the tributary and Channel. More evidence of this is seen in the left baseline on the Gamma Ray Logs for the three wells that lie within the channel. There is a shift to the right that increases in magnitude as we move from West to East among the three wells, again showing the trend moving northeast is becoming cleaner and finer grained.

Taken together, this information implies paleoenvironment interpretation. Remembering that as we move vertically along the log, we are getting younger in time, we will begin at the base. There are multiple fining upwards sequences that indicate flooding events, which allow heavier sediment to be transported and deposited. This is indicated on the logs with the bottom two blue dashed lines. As we reach the third blue dashed line, it seems as if these flooding events cease and the oscillatory motion becomes dominant, meaning that we have changed environments entirely. Most likely we have reached a point in time that is primarily showing transgressions and regressions of the shoreline at this specific location. Facies analysis studies conducted by KGS in Northern Kansas

indicates oscillatory GR behavior between shales and carbonates can interpreted as transgressive and regressive shoreline movements (Boggs, 2006).

Three of the four wells discussed here have indications of channel stratigraphy at the MP boundary. By precisely locating these wells on broad- and narrowband time slices we are lead to the conclusion that the 41 Hz time slice contains image features likely to represent subtle channel features that are not visible in the broadband data. We find there is in fact an extension off the main channel representing an incised valley. This is indicated by the successions of fining upwards sequences that are exhibited by the three wells that lie in or very near the channel and its extension. When these wells are compared to one that lies outside the reaches of these features, it can be seen that the logs show different environments between the two groups.

These interpretations coupled with previous work showing correlations between the narrow band data and the curvature and spice attributes allow me to determine that the narrow band channel feature represents a verifiable geological feature in the subsurface. We intend to pursuing analysis of other wells that lie farther away from both features to determine if the same patterns and conclusions hold.

Standard deviation first arrival theory

As part of undergraduate J. Seales training program, we have teamed up with a group in the Allied Geophysical Lab at the University of Houston who are making ultrasonic transmission measurements to estimate P and S wave speed in calibration material (aluminum). In this work, time-of-flight is used to estimate wave speed, but an important problem is accurate picking of the P-wave first arrival times and later S-wave arrival times. This work is funded by Geokinetics.

During a joint CO_2/AGL/Geokinetics meeting, Dr. Bernhard Bodmann suggested that one could determine first arrivals on seismic traces by computing standard deviation of noise levels in the data. The method he described uses the standard deviation of the noise (before signal arrival) in order to quantify the amount of amplitude stand-out that will be considered a signal arrival, and use this to locate P-wave first arrivals. To test this we constructed synthetic data with 225 time samples and amplitude variations simulating noise followed by signal arrivals (Figure 3), and then applied the proposed method.

Method:

1. Compute noise mean
2. Compute noise Standard Deviation
3. Divide entire trace amplitude by noise standard deviation, call this X
4. Correct for the calculated mean
5. Assign a new value Y using the following criteria
    a. If $-2 \leq X \leq 2$, then $Y = 0$
    b. If $2 \leq X$, then $Y = 1$
    c. If $X \leq -2$, then $Y = -1$
6. Find first occurrence where $Y \neq 0$, and this is our first p-wave arrival
7. Correlate this specific Y to its sample number and we have the arrival time

The synthetic noise values were analyzed and the mean was be found to be -0.38 and standard deviation = ±9.85. Figure 4 shows the ratio (X) of data amplitude and noise standard deviation calculated for each sample. This quantity was used to assign Y that is plotted in Figure 5. When this plot is zoomed in to see the first deviation from zero, Figure 6, the first break can be correlated to its sample number resulting in the first p-wave arrival time. If we then locate this sample on our wiggle plot of the values from Table 1, we can see there is a correct correlation with the first significant amplitude that would be associated with the first p-wave arrival (Figure 5). A detail plot of this result is given in Figure 6 and the original data with first arrival pick overlay is shown in Figure 7. From this test, we concluded the method was viable.

Our first test on lab data used a 100 kHz shear wave source. When transmission experiments are done, it is important to know the travel time between source and receiver when there is no material sample between them. This is called the direct contact time and is subtracted from later measurements as a correction. Computing Y as described above for the direct contact data resulted in Figure 8, shown zoomed in Figure 9. Comparison with manual first arrival picks of data traces showed the new picking method was able to consistently find the arrival as well or better than visual methods (Figure 10).

Next the new method was applied to data from a real sample of aluminum. Figure 11 shows the Y plot using a 2-sigma threshold designed to pick up the weak P-wave arrival. One early non-zero Y value is thought to be a noise spike and was ignored, but we are working on a method that would automatically bypass such spurious noise bursts. A detail plot of the P-wave first arrival is shown in Figure 12.

A secondary objective was picking of the S-wave arrival in this data, an event that comes in after the P-arrival and it's picking is complicated by various P and P-S (mode converted) events. Since the S arrival is a large amplitude event, we were able to automatically pick it by using a 10-sigma threshold in the Y computation. In this way, smaller amplitude P and P-S events were bypassed in favor of the high amplitude S event. Figure 15 shows the result of manual and automatic picking of both P and S arrivals in the 100 kHz aluminum data. There is room of improvement here, perhaps a 6-sigma threshold would do a better job with the S-wave. We will continue testing and improving this algorithm.

Acoustic finite difference modeling

Looking ahead to numerical modeling based on layer models from well logs, we performed tests related to numerical dispersion, a kind of undesirable noise or artifact that develops in numerical modeling of wave fields. The basis for our test was a 2D acoustic finite difference modeling program in the SeismicUnix (SU) processing system (Cohen, 2010). Specifically, we modified the XDemo5 tutorial for the finite difference modeling program sufdmod2. This demo contained a model of horizontal layers used to create an (x,z) earth model. The first step requires building a velocity and density model by using the SU program unif2. The standard inputs for

this program are:

```
unif2 < infile > outfile [parameters]
```

where the infile, outfile and parameters are listed in table 1. To view the constructed models, the SU program ximage was used with syntax

```
ximage n1= [optional parameters] <binaryfile
```

and all parameters are represented in Table 2. The modeling program itself (sufdmod2) was then run with input for this routine is as follows:

```
sufdmod2 <vfile >wfile nx= nz= tmax= xs= zs= [optional parameters]
```

where the inputs and parameters are outlined in Table 3.

After building and running all necessary models, the first result can be seen in Figure 16. A surface layer velocity of 4000 m/s (lowest velocity in the model) was used in this case resulting in strong numerical dispersion as noted on the plot. Such dispersion is occurs when the distance between adjacent nodes in the numerical grid are a significant fraction of the shortest wavelength in the simulated wavefield. One way to reduce dispersion is thus to increase the lowest velocity in the earth model as shown in Figure 17 (5000 m/s) and Figure 18 (6000 m/s). In each case, reflection time from the first interface is smaller as expected, but we can also see an accompanying improvement in the numerical dispersion.

While changing earth velocities is useful as an illustration of dispersion, it is not feasible to think of changing velocities in a real earth model. The alternative is to make a finer numerical grid (i.e., smaller node separation) since dispersion is caused by using a grid cell size that is too large.

The next task undertaken was to modify the grid, creating a grid cell (dx,dz) that was half the original while keeping overall model dimensions the same. The time step interval (dt) is changed internally by the program to maintain numerical stability. The first attempt finer-grid modeling is seen in Figure 19.

The result is reduction in numerical dispersion and the image has become sharper. Also, note the difference in scale on the vertical axis resulting in an appearance of a steeper arrival slope. To refine this image even more, another attempt was conducted as seen in Figure 20. This time, the goal was to set dx=dz=5m. Again, considerable improvement is seen in the image by decreasing the numerical dispersion.

Work Plan for the next quarter

Geology: Previously we were focusing on mainly deep carbonate section below the karst-modified unconformity. Next semester, we plan to focus on the application of seismic attributes to the fracture, lithology, and rock property interpretation/visualization of mixed clastic carbonate sequences. This is a current hot topic in seismic geomorphology and seismic sedimentology. This includes following:

1. Study of lithology, sedimentary facies in the shallower sections, and geological interpretation on confined or intra-strata features extracted by ANT. This needs to merge the two sections into a single model with the help of seismic and logs, also overcome the software defect in zone-correlation so that the facies/lithology study is within the correct stratigraphic framework.
2. Evaluate different statistical models in property gridding for clastics and carbonate, the efficiency of different seismic attributes to the interpretation and visualization of different features, such as lateral facies changes, vertical stacking within seismic resolution and detachability windows, structural features.
3. Work flows: If the deep and shallow section models can be merged into a single property grid, we plan to try the reservoir simulator in Petrel to see if it is possible to pipe all steps from data interpretation/analysis, to reservoir characterization, finally to reservoir simulation in the same platform. This can avoid errors during the data transfer between systems. A complete training course on "reservoir characterization and simulation" work flow can be developed from this step for teaching purposes.

Elastic modeling: Build more 1D elastic models for wells on other positions in Dickman I survey, then we can establish an optimal 3D elastic model. And generating pre-stack data to establish elastic seismic data volume by forward modeling. With the seismic data and the 3D velocity model, we will try elastic migration to get the subsurface image and to analyze footprint effect.

Flow to seismic: The 1D convolutional forward modeling has demonstrated its ability to image major subsurface featuress quite accurately, but is too simplistic to resolve the complex structure. As such, a more realistic forward modeling method is needed to perform a more accurate comparison for detecting the CO2 change at different time intervals. The new method will start with the utilization of 2D full wave forward modeling programs in Seismic Unix. These programs are *sufdmod2, suea2df* and *sufctanismod*. They represent elastic/acoustic anisotropic/isotropic forward modeling via finite difference approximations to the appropriate wave equation. The seismograms generated will have all types of waves (primary reflections, multiples, direct waves, etc.) and thus represent a more realistic earth response. The program *suea2df* includes anisotropy, and a shear wave velocity model is also one of input parameters for the elastic waves. As with convolutional forward modeling, the required parameters include the fluid saturated rock velocities and densities with numbers of samples in x, z direction (2D case), these will be kept the same as calculated by the formulas shown in the previous

reports. Other parameters include source average frequency, wavelet type, etc., these will be up to the user's preferences in different cases.

We will continue generating the new seismic datasets by the full forward modeling at different time intervals. The new flow simulation model will be used which shows the sequestration target in the Mississippian porous carbonate.

Ultra narrow band filtering: Work will continue toward validation of channel features in the 41 Hz narrow band data, and fracture indicators at 6 Hz.

Cost and milestone status

Baseline Costs Compared to Actual Incurred Costs….

1/1/10 – 3/31/10	Plan	Costs	Difference
Federal	$36,668	$26,352	$10.316
Non-Federal	$4,063	$0	$4,063
Total	$40,730	$26,352	$14,378

Forecasted cash needs Vs. actual incurred costs

Notes:
(1) Federal plan amount based on award of $293,342 averaged over 8 reporting quarters.
(2) Non-Federal plan amount based on cost share of $32,500 averaged as above.
(3) Cost this period reflects salary for C. liner (1 mo) and J. Seales (3 mo).

Actual Progress Compared to Milestones

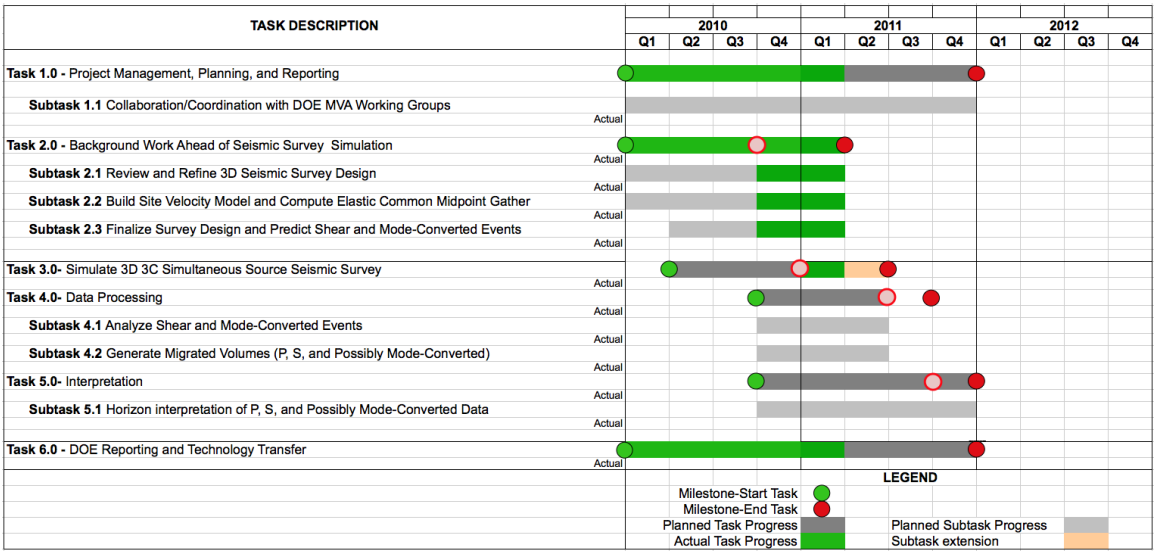

Personnel

Prof. Christopher Liner is Principle Investigator and lead geophysicist. He is a member of the SEG CO_2 Committee, Associate Director of the Allied Geophysical Lab, and has been selected to deliver the 2012 SEG Distinguished Instructor Short Course.

Dr. Jianjun (June) Zeng has been working exclusively on this project since Dec 2007 and is lead geologist.

Ms. Qiong Wu is a graduate PHD student in geophysics who joined the project in January 2010 as a research assistant. She will be funded year-round out of the project.

Mr. Johnny Seales is an undergraduate student majoring in Geology and Geophysics. He is also a U.S. Army veteran, having served in Iraq. He will be funded year-round from the project. He anticipates earning his undergraduate degree in Dec. 2011.

Ms. Jintan Li is a 3rd year PhD student in geophysics who joined the project in Aug 2009. She is funded by Allied Geophysical lab at this time. Her thesis will be time-lapse seismic modeling (4D) for conducting dynamic reservoir characterization of the Dickman Field.

Tim Brown is a graduate MS student working on low frequency fracture indicators.

Eric Swanson is a part-time graduate MS student working on amplitude interpretation at the Miss-Penn unconformity. He is a full time employee of Swift Energy.

Technology transfer activities

A CO_2 Sequestration Simulation Case Study at the Dickman Field, Ness Co., Kansas
Christopher Liner, Po Geng, Jianjun Zeng, Heather King and Jintan Li (SPE 2011)

Contributors

Christopher Liner	(P.I, Geophysics)
Jianjun (June) Zeng	(Geology and Petrel Modeling)
Po Geng	(Flow simulation)
Ph.D. students:	Qiong Wu, Jintan Li
MS students:	Tim Brown, Eric Swanson
BS student:	Johnny Seales

References

Boggs, S., 2006, Principles of sedimentology and stratigraphy, 4th Edition: Pearson Education, Inc.

Cohen, J. K. and Stockwell, Jr. J. W., (2010), CWP/SU: Seismic Un*x Release No. 42: an open source software package for seismic research and processing, Center for Wave Phenomena, Colorado School of Mines.

Tables

Velocity Model		
Symbol	**Value**	**Explanation**
	model.unif2	File read in
nx	1250	number of x samples (2nd dimension)
nz	2500	number of z samples (1st dimension)
dx	2	x sampling interval
v00	5000,5500,6000,6500, 7000,7500,8000	velocity at each x0, z0 (m/sec)
dz	2	z sampling interval
	velocity.1	file created
Density Model		
Symbol	**Value**	**Explanation**
	model.unif2	File read in
nx	1250	number of x samples (2nd dimension)
nz	2500	number of z samples (1st dimension)
dx	2	x sampling interval
v00	1.0,2.25,2.25,2.25,2.35,2 .35,2.35	velocity at each x0, z0 (g/cc)
dz	2	z sampling interval
	density.1	file created

Table 1. Input files and parameters for velocity and density models.

Viewing the Velocity Model		
Symbol	**Value**	**Explanation**
	velocity.1	File read in
title	"velocity profile"	title of plot
legend	1	display the color scale
xbox	10	x in pixels of upper left corner of window
ybox	10	y in pixels of upper left corner of window
n1	2500	number of samples in 1st (fast) dimension
n2	1250	number of samples in 2nd (slow) dimension
d1	2	sampling interval in 1st dimension
d2	2	sampling interval in 2nd dimension
Viewing the Density Model		
Symbol	**Value**	**Explanation**
	density.1	file read in
title	density profile	title of plot
legend	1	display the color scale
xbox	750	x in pixels of upper left corner of window
ybox	10	y in pixels of upper left corner of window
n1	2500	number of samples in 1st (fast) dimension
n2	1250	number of samples in 2nd (slow) dimension
d1	2	sampling interval in 1st dimension
d2	2	sampling interval in 2nd dimension

Table 2. Input files and parameters for viewing the velocity and density models.

Finite Difference Modeling		
Symbol	**Value**	**Explanation**
<vfile	velocity.1	file containing velocity (nx) (nz)
>wfile	cube.out	Wavefield snapshot file (nx) (nz)
nx	1250	numbe of x samples (2nd dimension)
nz	2500	number of z samples (1st dimension)
xs	0	x coordinates of source
zs	100	z coordinates of source
tmax	12	maximum time
dx	2	x sampling interval
dz	2	z sampling interval
dfile	density.1	input file containing density (nx) (nz)
fmax	80	maximum frequency in source wavelet
nt	3001	number of time samples (dt determined for stability)
hsz	10	z coordinate of shot record
hsfile	shot.su	Shot record output file (nx) (nt)
abs	0,1,1,1	free surface condition on the top
verbose	2	more messages
mt	10	number of time steps per output time step

Table 3. Inputs and parameters for building the finite-difference model.

Figures

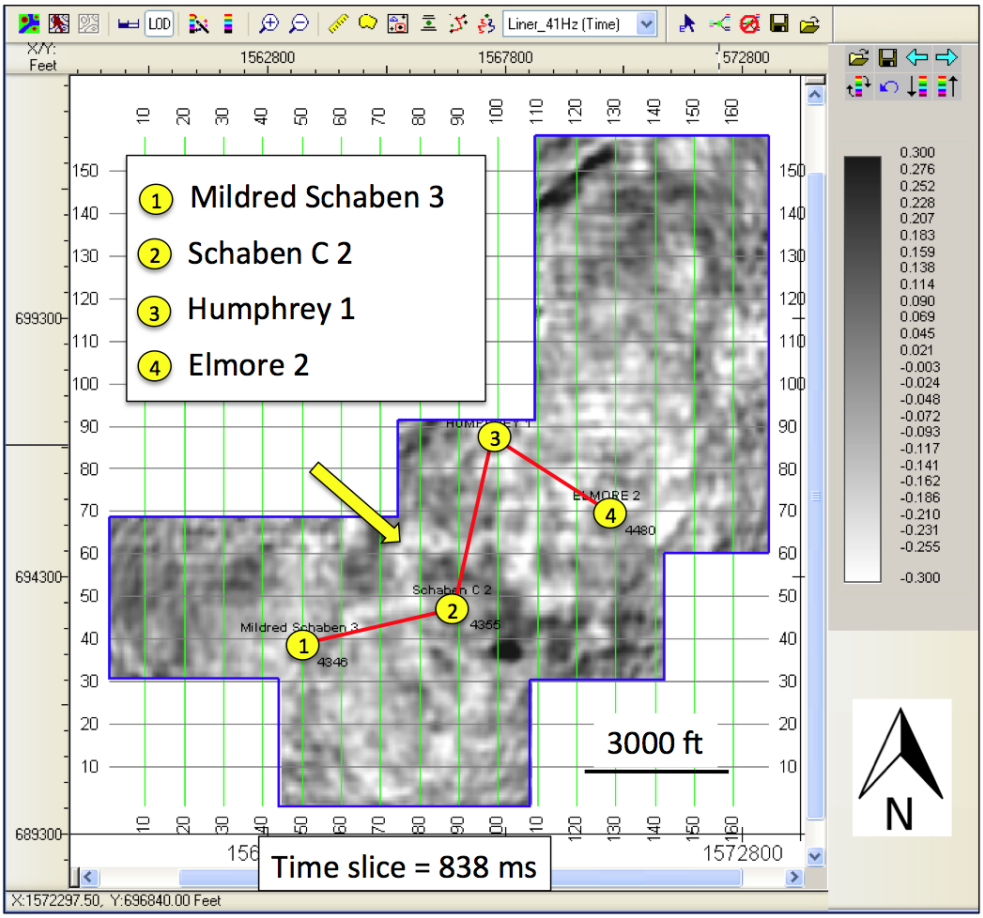

Figure 1: Narrow-band (41 Hz) ime slice showing the location of four wells used to interpret channel extension. Yellow arrow highlights suspected channel.

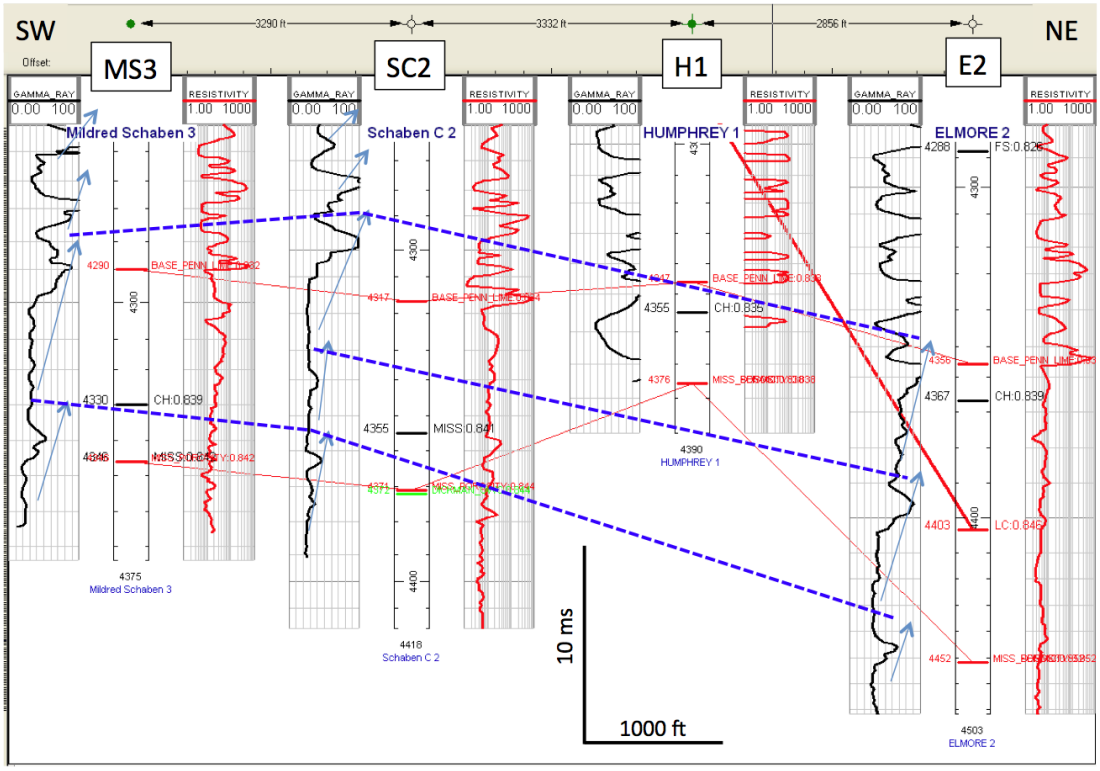

Figure 2. Four wells that compose our cross section line from Fig. 1. The two logs present for each well are Gamma on the left and Resistivity on the right. Correlation lines (solid red and blue dash) and fining upward sequences (blue arrows) are shown.

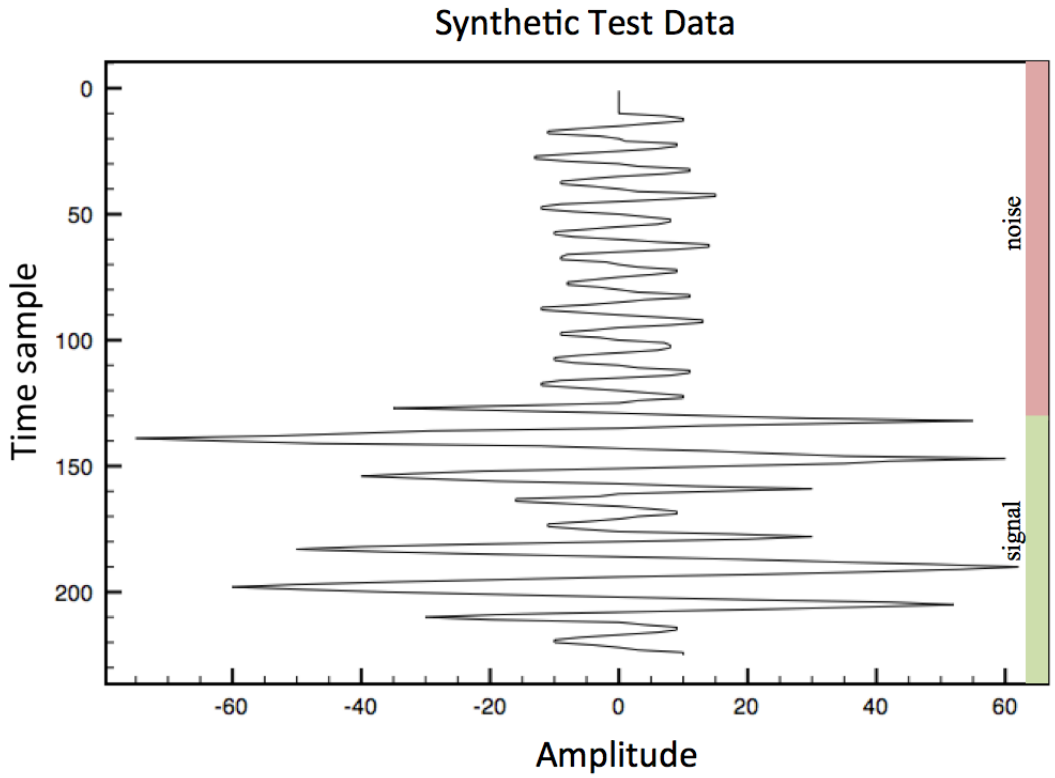

Figure 3. Wiggle plot of synthetic data used to develop first break picking algorithm.

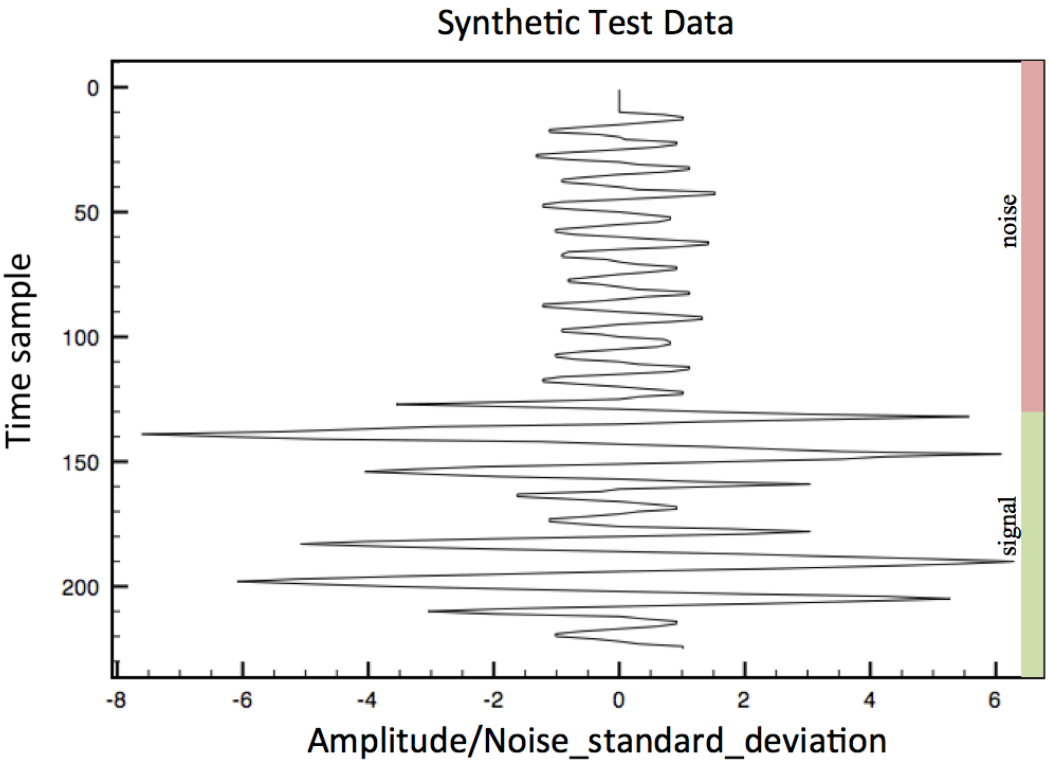

Figure 4. Computed ratio of noise standard deviation to amplitude of synthetic data.

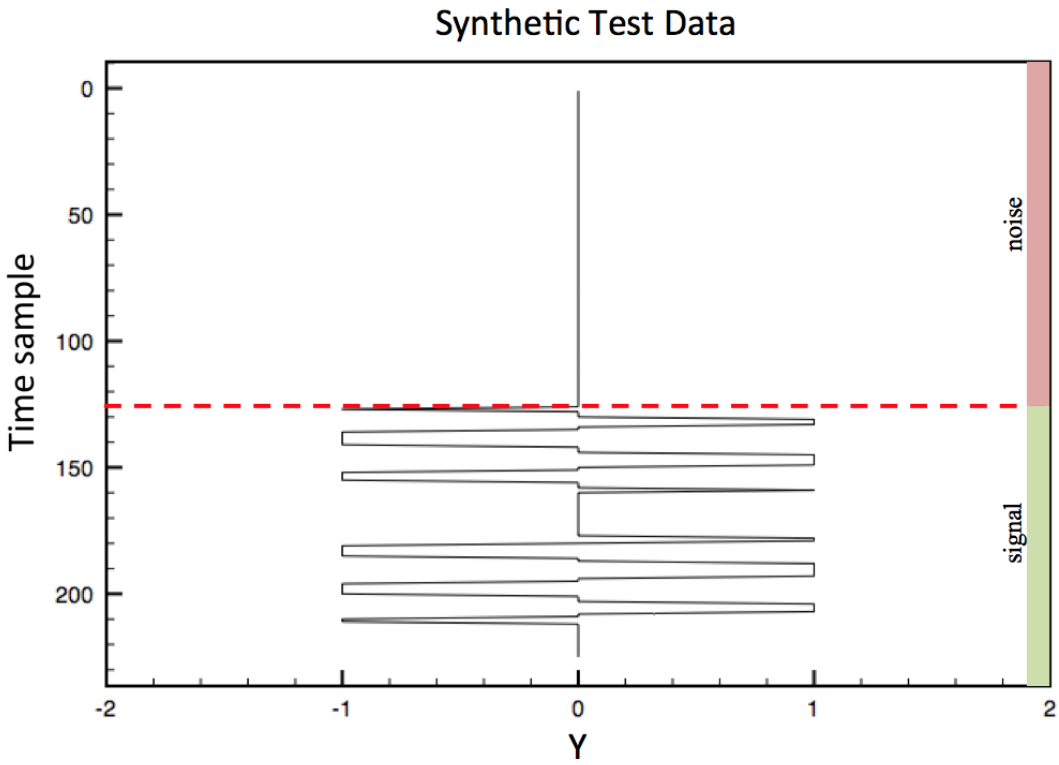

Figure 5. First arrival measure Y is a threshold value computed from amplitude divided by noise standard deviation (X). If X lies in the interval [-2,2] then Y is assigned a value of zero, otherwise, Y is -1 or +1. This is a 2-sigma statistical limit.

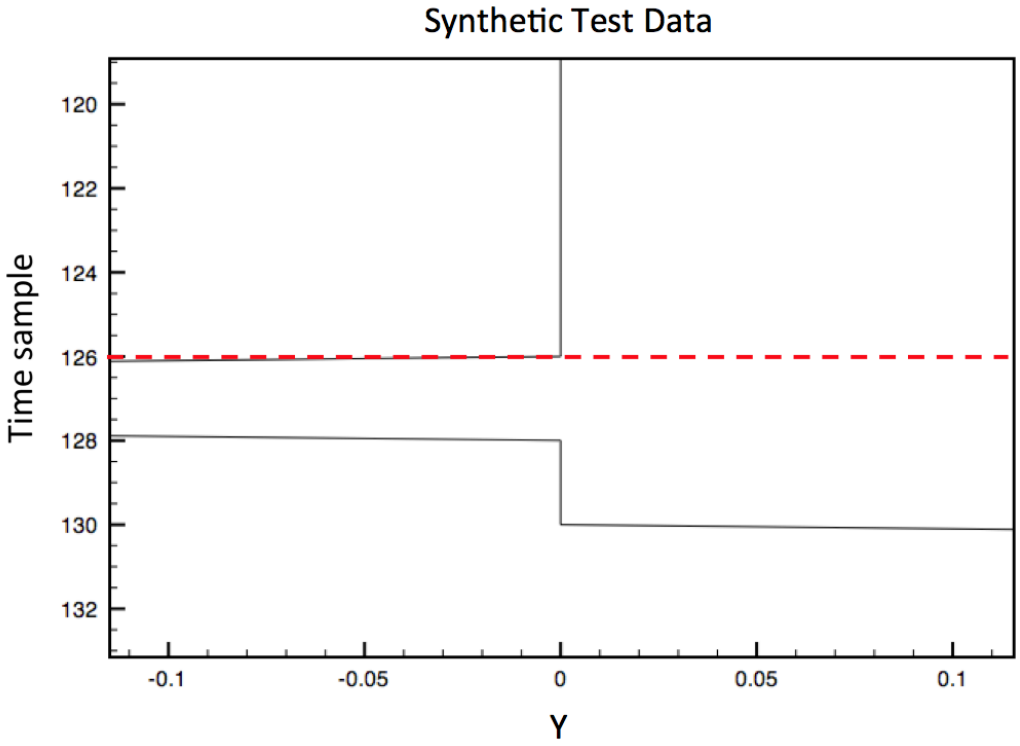

Figure 6. Detail view of first arrival pick (red dash) from computed Y values.

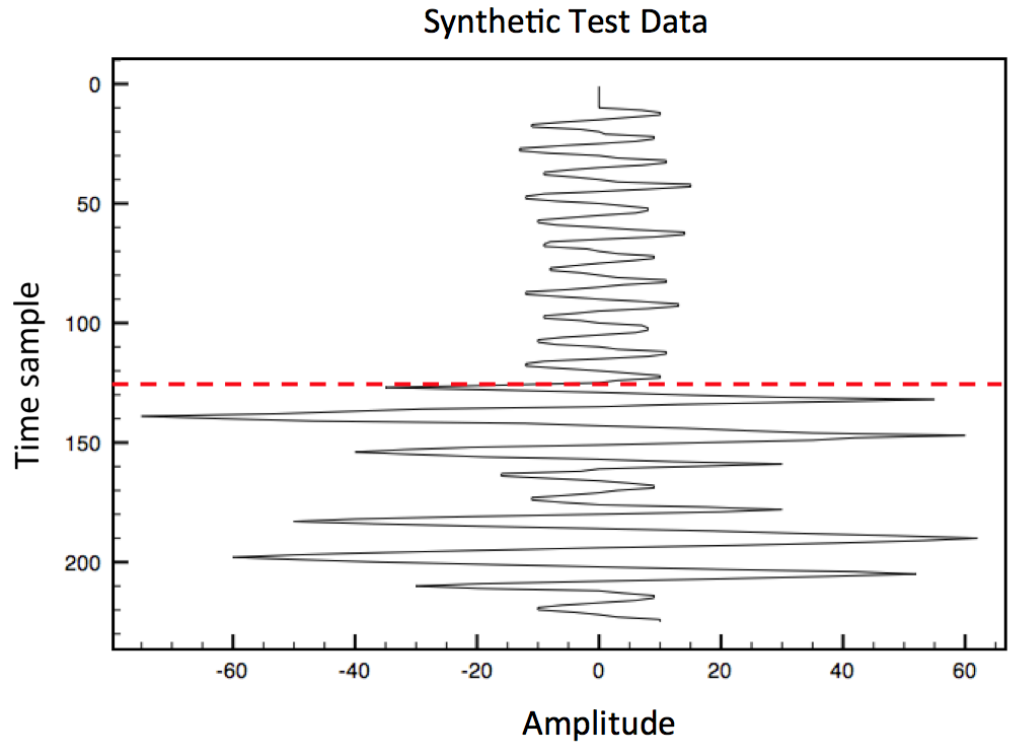

Figure 7. First arrival pick displayed on original synthetic data.

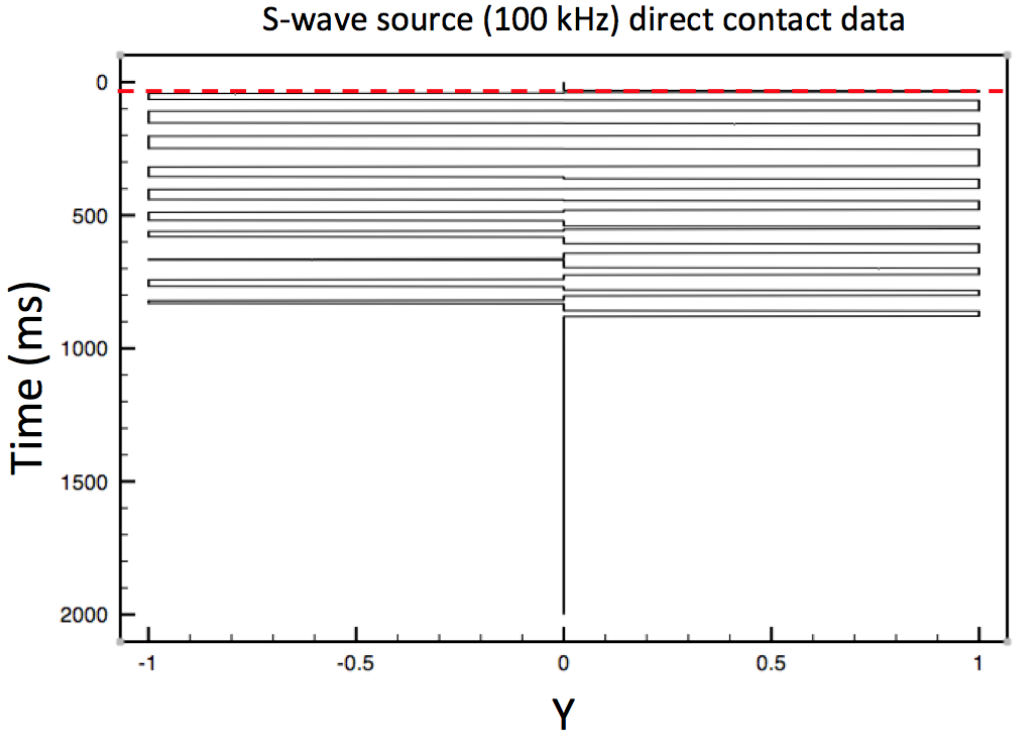

Figure 8. 100 kHz S-wave source direct contact Y plot with first arrival (red dash).

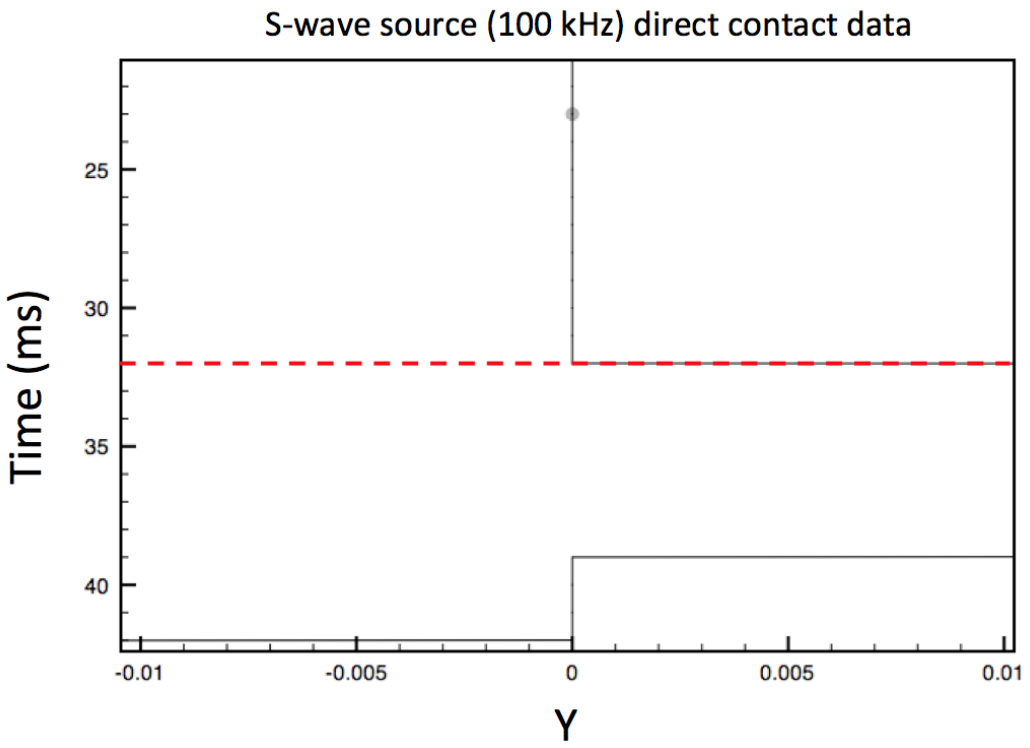

Figure 9. Detail of direct contact first arrival pick (red dash) for 100 kHz S-wave source.

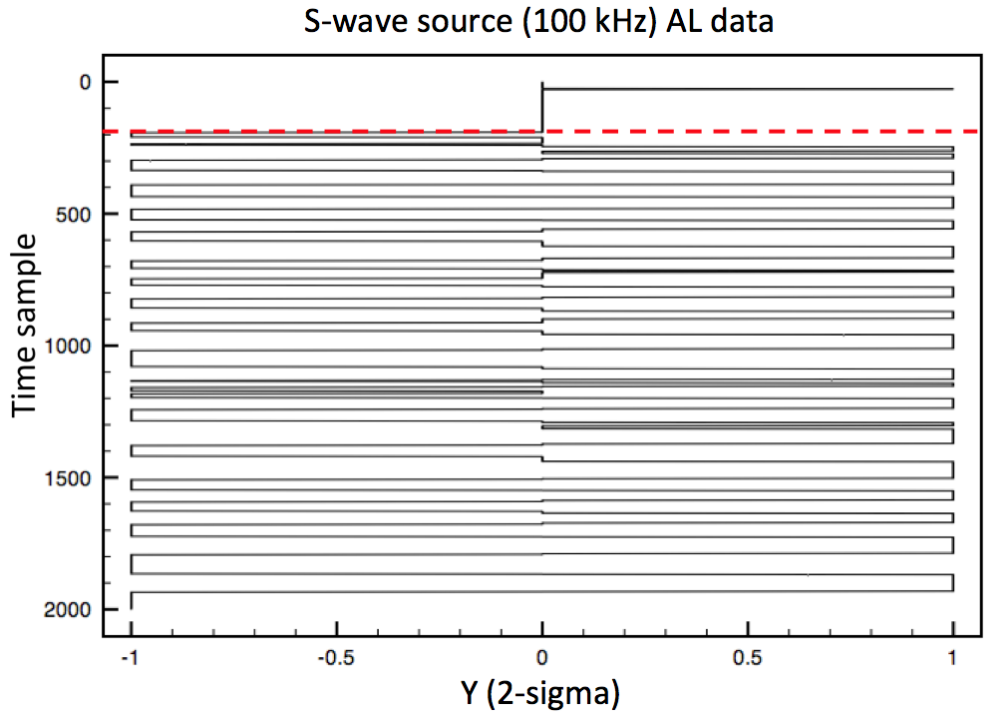

Figure 11. Aluminum transmission data after standard deviation processing.

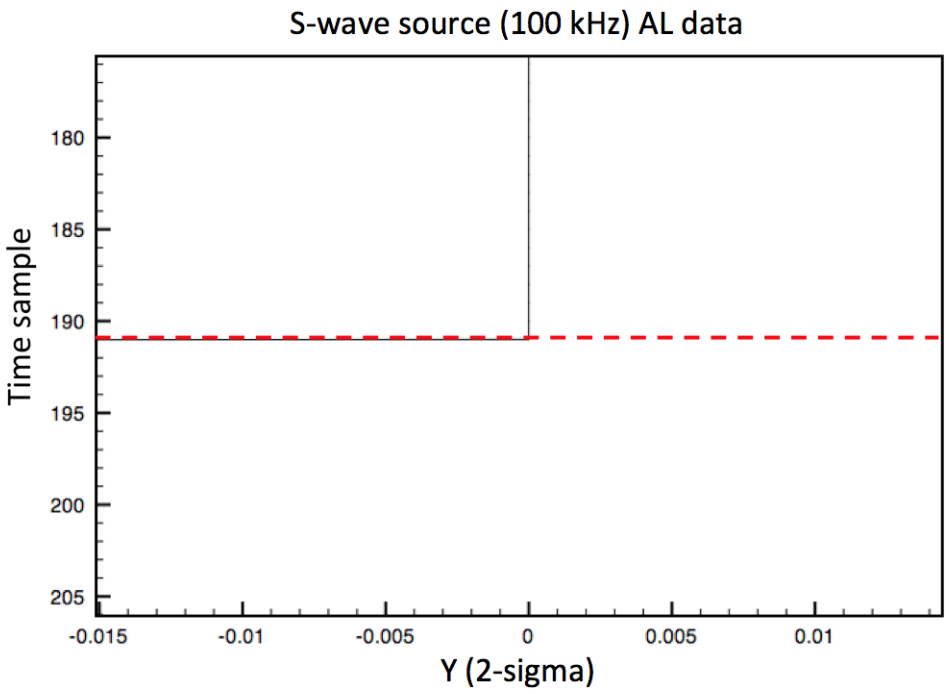

Figure 12. Aluminum transmission detail plot with P-wave first arrival pick (red dash).

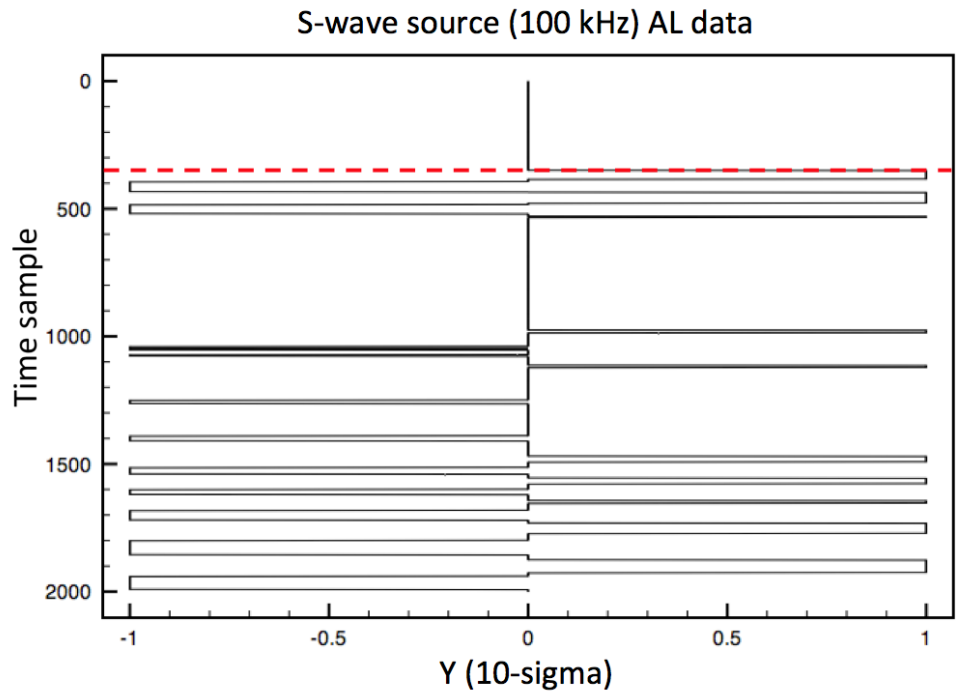

Figure 13. Aluminum data Y plot with 10-sigma threshold used for picking the high-amplitude shear wave arrival.

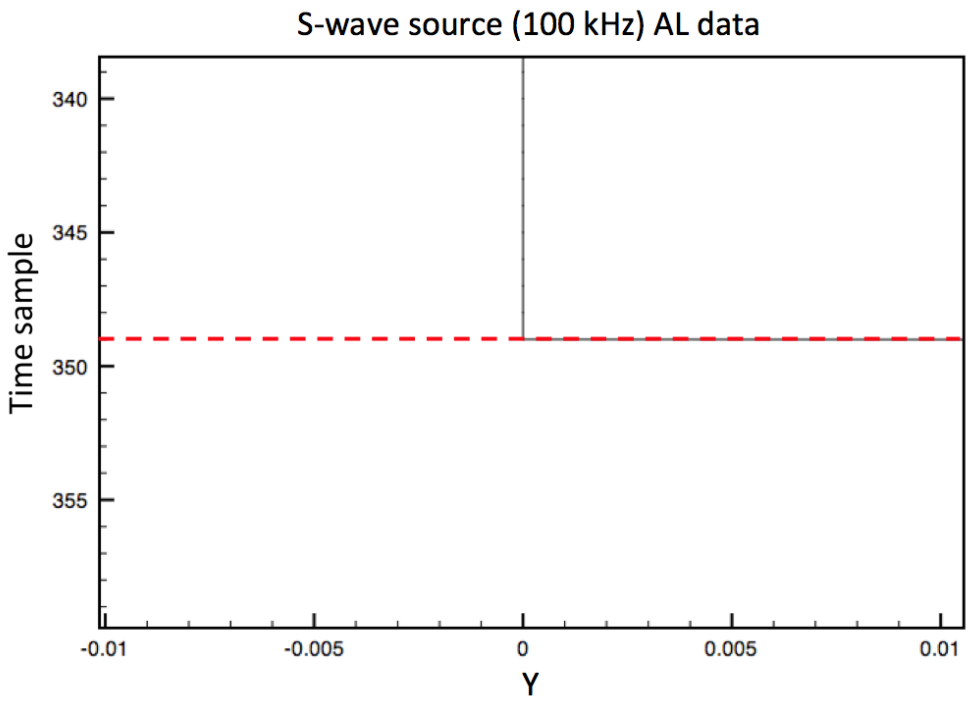

Figure 14. Detail of aluminum data Y plot with 10-sigma threshold used for picking the high-amplitude shear wave arrival.

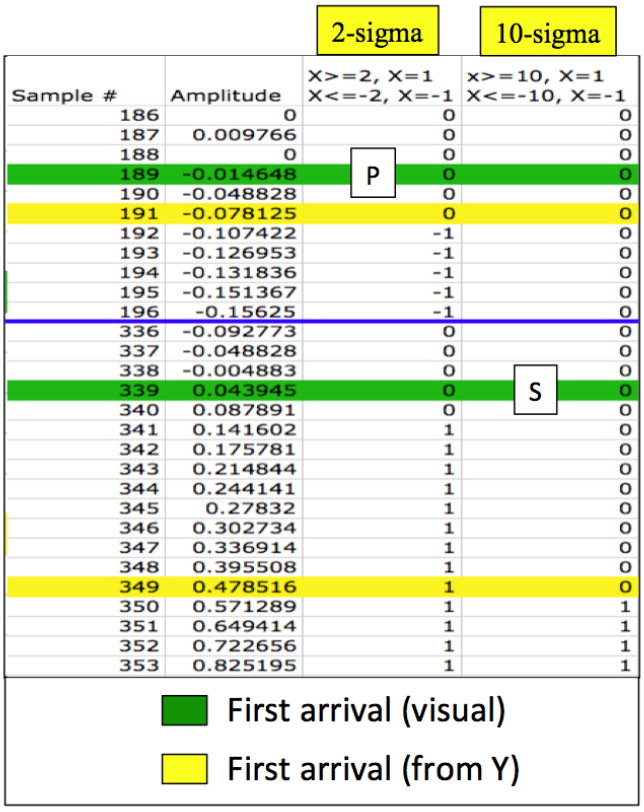

Sample #	Amplitude	X>=2, X=1 X<=-2, X=-1	x>=10, X=1 X<=-10, X=-1
186	0	0	0
187	0.009766	0	0
188	0	0	0
189	-0.014648	0	0
190	-0.048828	0	0
191	-0.078125	0	0
192	-0.107422	-1	0
193	-0.126953	-1	0
194	-0.131836	-1	0
195	-0.151367	-1	0
196	-0.15625	-1	0
336	-0.092773	0	0
337	-0.048828	0	0
338	-0.004883	0	0
339	0.043945	0	0
340	0.087891	0	0
341	0.141602	1	0
342	0.175781	1	0
343	0.214844	1	0
344	0.244141	1	0
345	0.27832	1	0
346	0.302734	1	0
347	0.336914	1	0
348	0.395508	1	0
349	0.478516	1	0
350	0.571289	1	1
351	0.649414	1	1
352	0.722656	1	1
353	0.825195	1	1

Figure 15. Comparison of using 2-sigma versus 10-sigma threshold for first arrival picks.

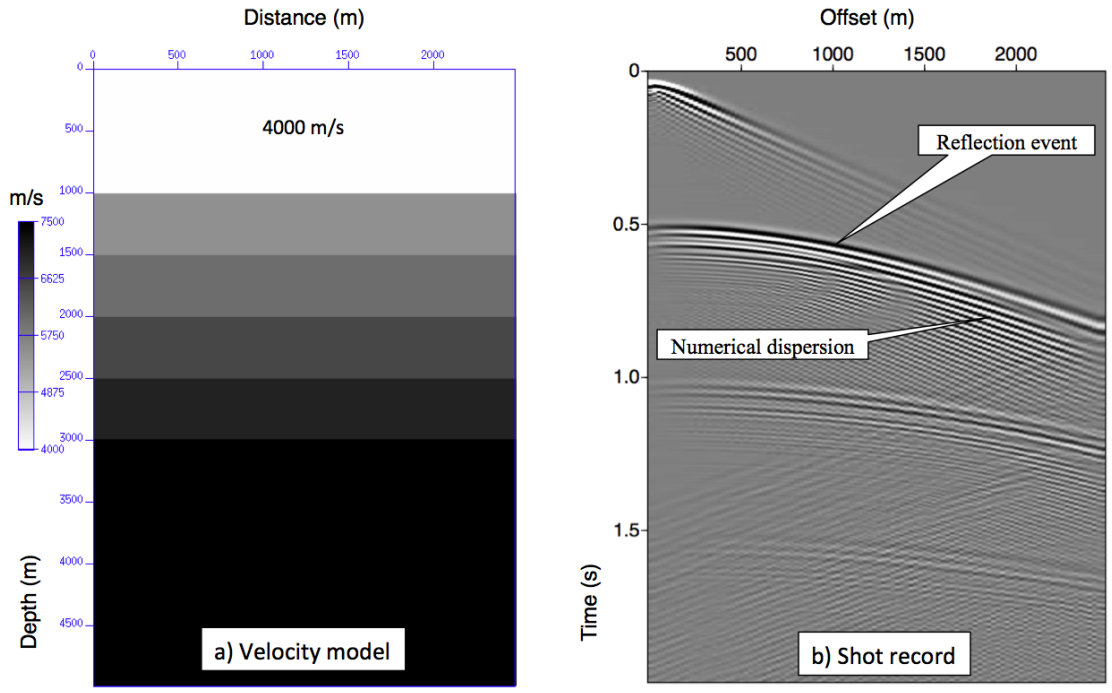

Figure 16. Acoustic finite difference numerical dispersion study. (a) Layered velocity model with surface velocity of 4000 m/s. (b) Synthetic shot record with highlighted reflection event and numerical dispersion.

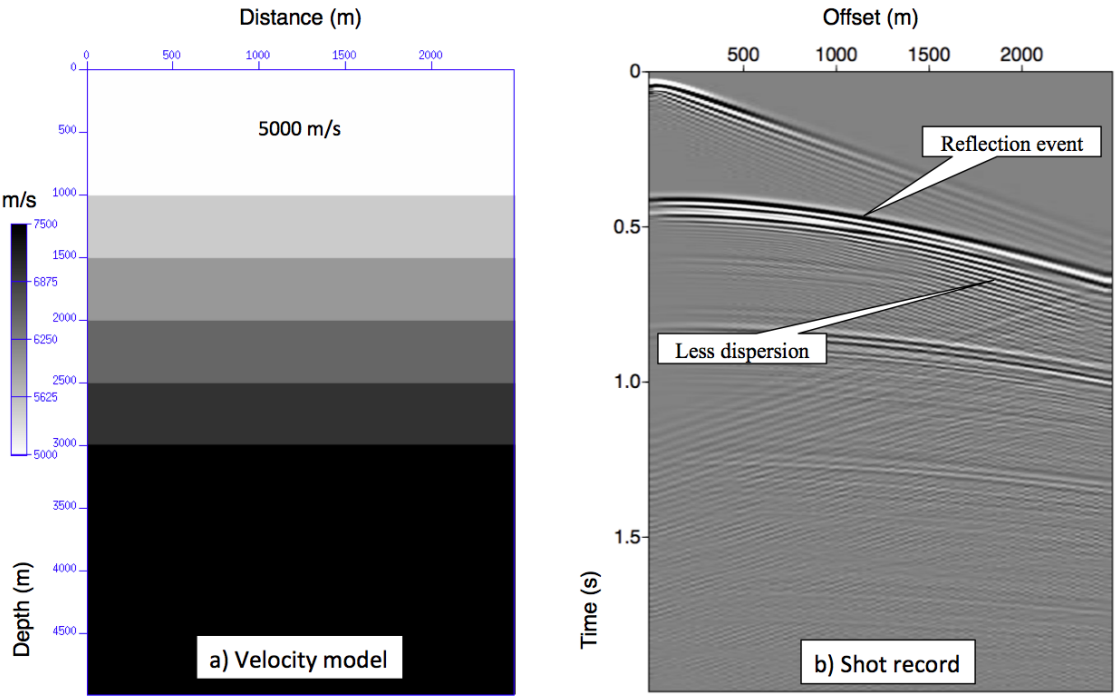

Figure 17. Acoustic finite difference numerical dispersion study. (a) Layered velocity model with surface velocity of 5000 m/s. (b) Synthetic shot record with highlighted reflection event and numerical dispersion.

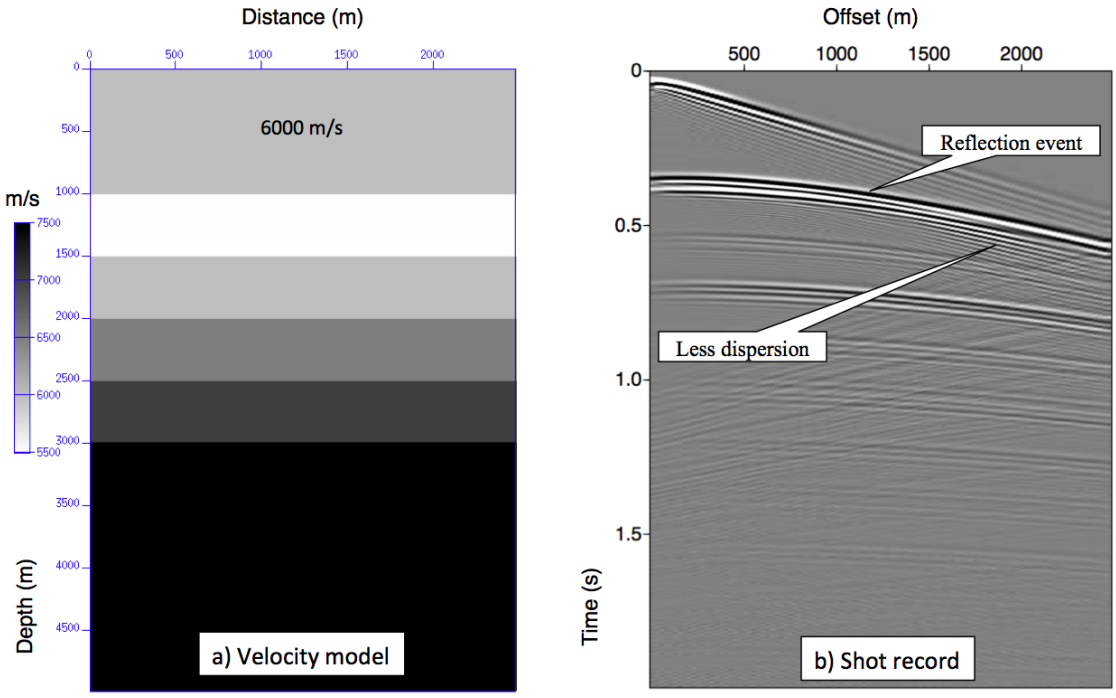

Figure 18. Acoustic finite difference numerical dispersion study. (a) Layered velocity model with surface velocity of 6000 m/s. (b) Synthetic shot record with highlighted reflection event and numerical dispersion.

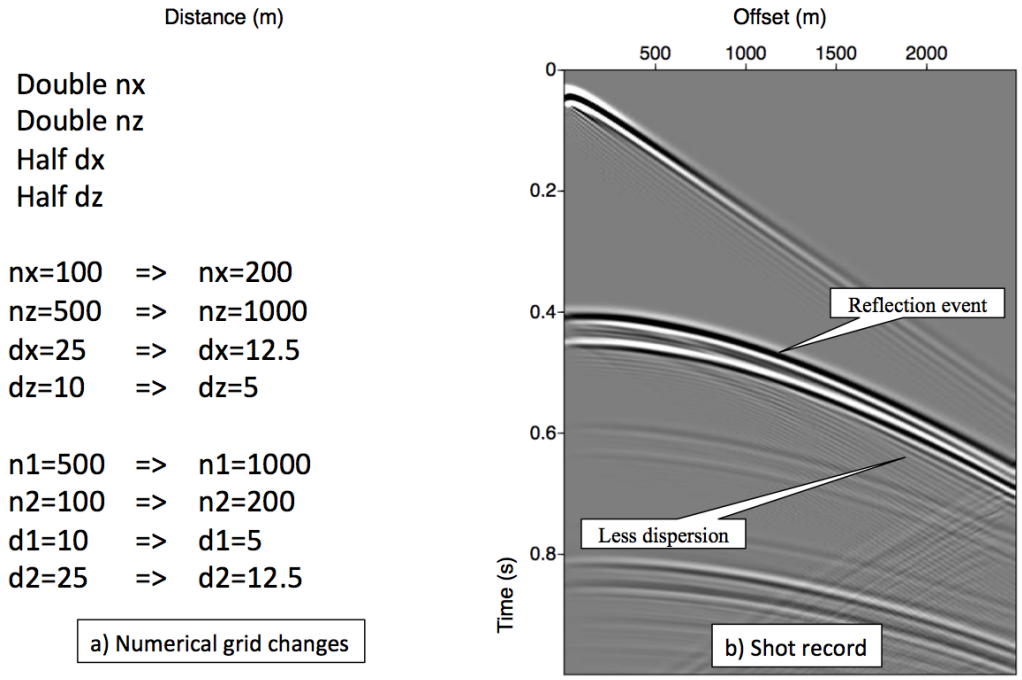

Figure 19. Acoustic finite difference numerical dispersion study with surface velocity of 5000 m/s. (a) Changes to numerical grid to reduce dispersion. (b) Synthetic shot record with highlighted reflection event and numerical dispersion.

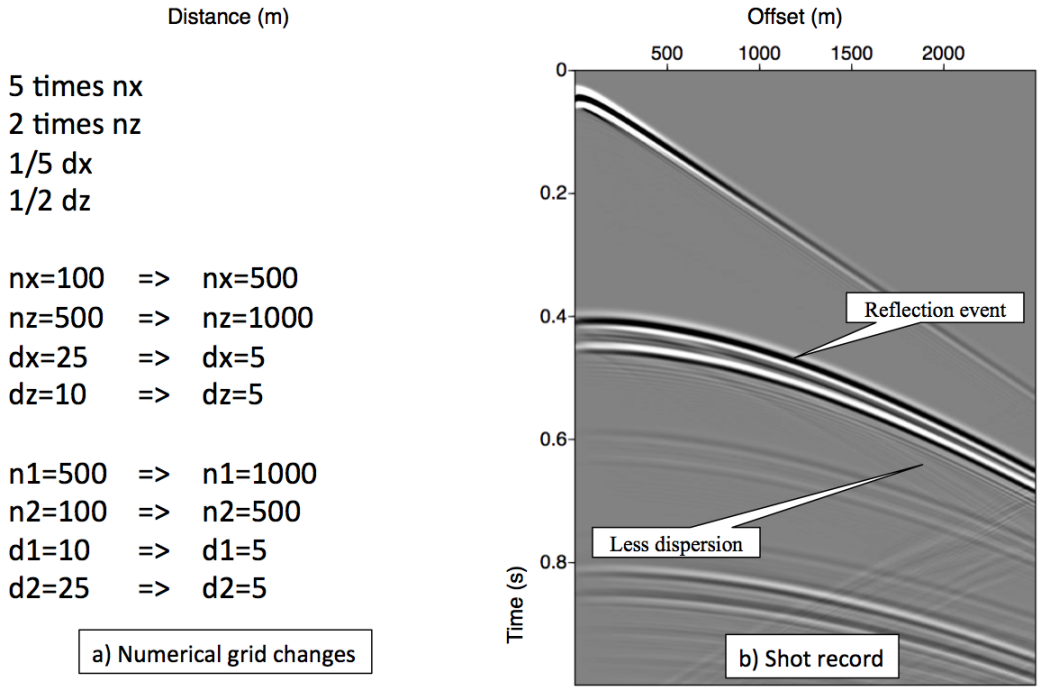

Figure 20. Acoustic finite difference numerical dispersion study with surface velocity of 5000 m/s. (a) Changes to numerical grid to reduce dispersion. (b) Synthetic shot record with highlighted reflection event and numerical dispersion.